Int. J. Electrochem. Sci., 11 **(2016)** 8964 – 8971, doi: 10.20964/2016.11.61

International Journal of
ELECTROCHEMICAL
SCIENCE
www.electrochemsci.org

Short communication

Facile Preparation of 1D α-MnO_2 as Anode Materials for Li-ion Batteries

Hongdong Liu[1], *Zhongli Hu*[1], *Yongyao Su*[1], *Rong Hu*[1], *Liangliang Tian*[1], *Lei Zhang*[2,*], *Haibo Ruan*[1,*]

[1] Research institute for new materials technology, Chongqing university of arts and sciences, Chongqing 402160, PR China
[2] College of life science, Chongqing normal university, Chongqing 401331, PR China
[*]E-mail: leizhang0215@126.com, rhbcqu@aliyun.com

Received: 15 July 2016 / *Accepted:* 13 September 2016 / *Published:* 10 October 2016

Manganese dioxide (MnO_2) has been studied as an anode material for Li-ion batteries beyond its high theoretical specific capacity and low-cost. In this work, the 1D α-MnO_2 nanomaterials with different morphology were synthesized via a facile and green hydrothermal method. These materials are carefully investigated by XRD, Raman, SEM and BET techniques. The results show that the solution acidity strongly influenced the morphology and the specific surface area of the sample. The electrochemical behaviors of MnO_2 sample were systematically investigated by cyclic voltammetry and galvanostatic charge-discharge. As anode materials for Li-ion batteries, both of 1.2-MnO_2 and 3.6-MnO_2 deliver high initial discharge capacity and relatively excellent cycle performance, indicating that 1D α-MnO_2 is a promising anode material for high-performance lithium ion batteries.

Keywords: α-MnO_2, solution acidity, Li-ion batteries, electrochemical performance

1. INTRODUCTION

In the past decades, Li-ion batteries are attracting much attention owing to their high energy density and long life, which render them intensively pursue for many promising candidates in energy storage and conversion, for instance electric vehicles, hybrid electric vehicles, laptops, and other portable electronic equipments[1-3]. However, the low theoretical specific capacity of graphite in commercial Li-ion batteries hinders its extensive applications especially for high energy and power energy storage systems[4, 5]. Therefore, new anode materials with high theoretical specific capacity are required to address these issues[6, 7].

Here, manganese dioxide (MnO_2) has been attracting tremendous attentions as an exception anode material with the desire to integrate such unique properties as high theoretical specific capacity of up to 1230 mA h g^{-1}, low price, natural abundance and environmental friendliness[8, 9]. MnO_2 has five main crystallographic structures : α, β, δ, γ, and λ[10, 11], and the polymorphs importantly contribute to Li-ion batteries performance. Among these crystallographic structures, α-MnO_2 shows relatively excellent electrochemical performance for Li-ion batteries due to it has a [2×2] tunnel structure which in favor of Li^+ transport in the materials. However, in previous reports, MnO_2 is usually brittle with significant capacity fading and large volume expansion, which is a challenge to meet the continuous energy demand[12, 13]. One effective approach for improving electrochemical performance of MnO_2 is to fabricate 1D MnO_2 nanostructures, such as nanowires, nanofibers, nanotubes, and nanorods, because the 1D nanostructure with high specific surface area could be facilitate the penetration of electrolyte, short the Li ion diffusion pathway and buffer the volume expansion[14, 15]. However, the previous reports are mainly on the MnO_2 as cathode material for lithium ion batteries[16-18].

Herein, we report a facile and green approach to synthesis 1D α-MnO_2 through the hydrothermal method. When evaluated as anode materials, both of 1.2-MnO_2 and 3.6-MnO_2 electrodes show high initial discharge capacity and relatively excellent electrochemical performance, indicating that 1D α-MnO_2 is a promising anode material for high-performance lithium ion batteries.

2. EXPERIMENTAL

2.1 Synthesis of MnO_2 nanostructures

The chemical reagents of potassium permanganate ($KMnO_4$, 99.9%, Shanghai Aladdin reagent Co., Ltd, China) and ethanol (C_2H_6O, 99.7%, Chengdu Kelong reagent Chemical Co., Ltd, China) were of analytical grade and used as purchase without any further purification. Hydrochloric acid (HCl, 36~18%, Chengdu Kelong reagent Chemical Co., Ltd, China) is diluted into the diluted HCl (3 M) before used.

MnO_2 nanostructures were synthesized by hydrothermal method using HCl as the reducing agent and $KMnO_4$ as the precursor. In a typical synthesis, 0.316 g of $KMnO_4$ was dissolved in 30 mL of de-ionized water with vigorous stirring for about 10 min. Subsequently, HCl solution was dissolved in the resulting solution by stirring for 10 min. Next, the resulting solution was sealed in a 50 mL Telfon-lined autoclave and hydrothermally treated at 160 °C. Finally, the as-prepared sample was centrifuged and washed with ethanol, which was followed by drying at 60 °C.

2.2 Material characterization

The phase components and crystal structure of the as-prepared samples were analyzed by XRD (TD-3500X) with Cu Kα radiation operating at 30 kV, 20 mA. The Raman spectra were recorded on a LabRAM HR800 Laser Confocal Micro-Raman Spectroscopy with 532 nm solid laser as excitation

source. The morphology and microstructure were characterized using scanning electron microscopy (SEM, FEI Quanta 250). The Brunauer–Emmett–Teller (BET) surface area and Barrett-Joyner-Halenda (BJH) pore size distribution were determined using Belsorp II surface area and porosity analyzer.

2.3 Electrochemical measurements

Working electrodes were prepared by mixing active samples, acetylene black, and polyvinylidene fluoride (PVDF) in N-methy-2-pyrrolidone (NMP) at a weight ratio of 80:10:10, respectively. Pure lithium foils were used as counter and reference electrodes. The electrolyte was 1 M $LiPF_6$ in ethylene carbonate (EC) and dimethyl carbonate (DMC) (1:1 v/v) mixture. All the 2032-type coin cells were assembled in an Ar-filled glove box. Cyclic voltammetric (CV) tests were conducted using a CHI760E electrochemical workstation. Galvanostatic charge and discharge cycling experiments were carried out a Neware battery tester (BTS-610) at a current density of 100 mA g^{-1} in a voltage range of 0.01~3.00V.

3. RESULTS AND DISCUSSION

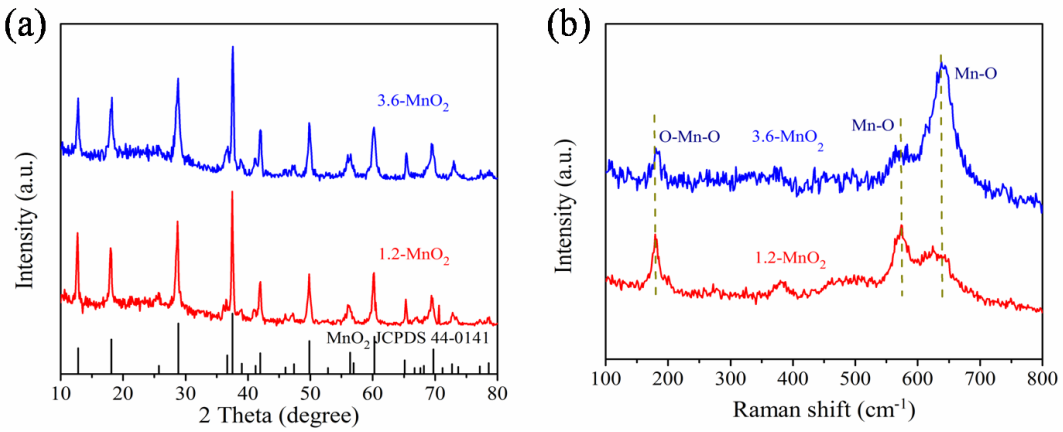

Figure 1. XRD patterns **(a)** and Raman spectras **(b)** of 1.2-MnO_2 and 3.6-MnO_2.

The crystallographic structure of the products were further identified by X-ray diffraction (XRD) as presented in Fig1(a), and the standard pattern of α-MnO_2 also shown in Fig1(a) for comparison. For 1.2-MnO_2 and 3.6-MnO_2 samples, all the diffraction peaks can be readily indexed to the tetragonal structure MnO_2 (α-MnO_2, JCPDS no. 44-0141) by comparing with the standard pattern. The sharp peaks with a high intensity indicate the highly crystalline and the relatively small nanocrystal size of the MnO_2 material. Besides, no diffraction peaks corresponding to impurity are observed, which indicates that the synthesized products with high purity. Remarkably, with the increase of HCl content in the precursor, the peak intensity of the crystalline MnO_2 has no obviously

change of the two samples. According to the Scherrer formula, the crystal sizes can be calculated to 17.7 nm and 14.9 nm, respectively. Furthermore, both 1.2-MnO_2 and 3.6-MnO_2 were characterized to further understand the crystal structure by Raman spectroscopy. As shown in Fig1(a), for all the two samples, the three evident characteristic Raman peaks centered at 383, 572, and 630 cm^{-1}, are assigned to the O-Mn-O stretching vibration, Mn-O stretching in basal plane of the MnO_6 sheet and Mn-O symmetic stretching vibration of the MnO_6 group double chains of MnO_2, respectively[19-21]. It is also evident that both of the samples have the crystal structure of the α-type MnO_2, which is in good agreement with the XRD result.

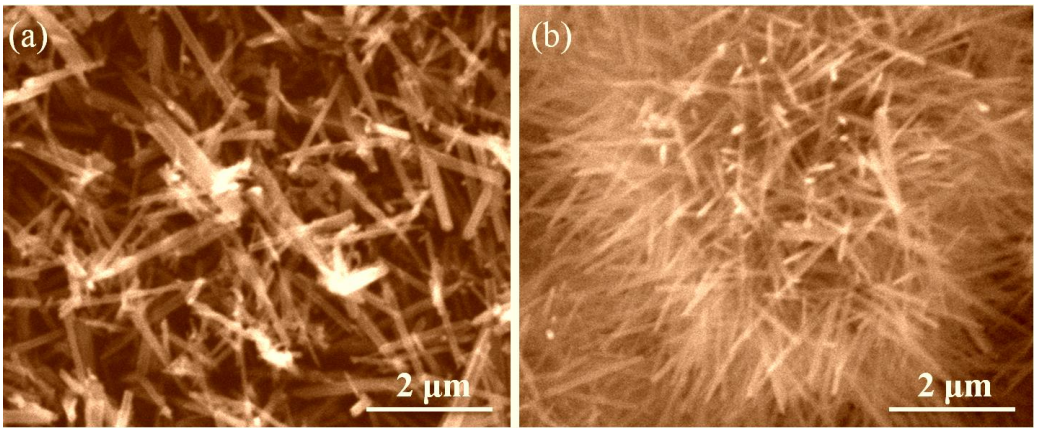

Figure 2. SEM images **(a)** 1.2-MnO_2 and **(c)** 3.6-MnO_2.

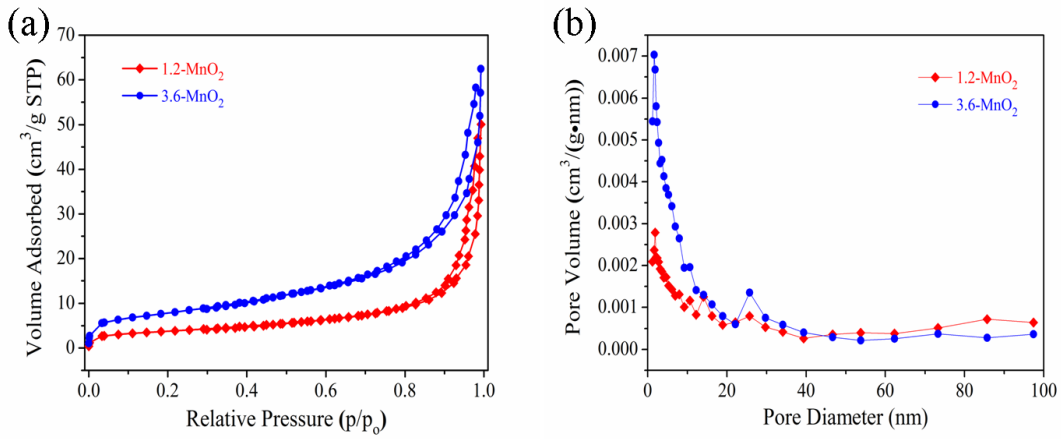

Figure 3. Nitrogen adsorption–desorption isotherms **(a)** and the corresponding pore size distribution curves **(f)** of the MnO_2 samples.

The morphology and microstructure of the as-prepared MnO_2 materials were investigated by SEM and TEM. As revealed by the SEM image (Fig2(a)), the 1.2-MnO_2 sample displays a uniformly nanotube structures and the nanotube with a length of more than 2 μm and a width of about 80 nm. Interestingly, the individual MnO_2 nanotube is likely to interconnect with each other. The SEM image of 3.6-MnO_2 in Fig2(b) shows the sample has a well-defined and hedgehog structures (~6 μm in

diameter), and the hedgehog composed of a large number of uniformly nanorods which stretch together along different directions. The nanorods with thick root and tapering outward has a ~2 μm long. Compared to the two samples, it is can be observed that the length and width of the nanorods are smaller than the nanotubes, suggesting the solution acidity strongly influence the growth of MnO_2 nuclei.

The specific surface area and pore size distribution of the MnO_2 materials were analyzed by N_2-sorption at 77 K. Typical IUPAC IV type adsorption–desorption isotherms with type H3 hysteresis loops are observed in Fig3(a), indicating that samples are mesoporous materials. Based on the Brunauer–Emmett–Teller (BET) analysis, the specific surface areas of the samples are calculated to be about 13.34 $m^2 g^{-1}$ and 27.75 $m^2 g^{-1}$, while the total pore volume is around 0.067 $cm^3 g^{-1}$ and 0.083 $cm^3 g^{-1}$, respectively. According to the Barrett-Joyner-Halenda (BJH) pore size distribution curves (Fig3(b)), both of 1.2-MnO_2 and 3.6-MnO_2 have broad pore-size distribution (micropores to mesopores) and the mean pore sizes are 20.20 nm and 11.91 nm, respectively. As the increases the HCl content, the specific surface area increases and the mean pore size gradually decreases, which can be interpreted as a consequence of the growth of the MnO_2 nuclei limited under high acidity. Importantly, this higher surface area, larger pore volume and smaller mean pore size, which may allow an efficient contact of MnO_2 with the electrolyte and result in the 3.6-MnO_2 with excellent electrochemical performance than the 1.2-MnO_2.

Fig4(a) and Fig4(b) show the first three CV curves of the 1.2-MnO_2 and 3.6-MnO_2 electrodes in a voltage range of 0.01~3.0 V at a scan rate of 0.2 mV s^{-1}, respectively. It can be seen that the shapes of the CV curves for the four samples are similar, indicating that the reduction and oxidation process of the as-prepared MnO_2 samples are consistent. As seen in Fig4(a), the two peaks at 2.32 V and 1.02 V in the first cathodic scan, which may arise from the formation of a solid electrolyte interface (SEI) layer and the reduction of MnO_2 into Mn, respectively[11, 22]. The obvious oxidation peaks cenctered at 1.23 V in the first anodic scan is characteristic of the oxidation of Mn to MnO_2[13, 23]. Apparently, in the subsequent cycles, the cathodic peak shifts significantly to lower volatge and anodic peak shifts to higher volatge, indicating the 1.2-MnO_2 has intensely polarization effect during the intercalation/deintercalation process. For 3.6-MnO_2 electrode (Fig4(b)), two cathodic peaks appear at 1.36 V and 0.95 V in the first cathodic process, and a broad anodic peak locat at 1.14 V in the first anodic process. In the following two cycles, a pair of cathodic/anodic peaks at 1.7/2.0 V and the peaks are stable, indicating the highly reversible redox reactions of 3.6-MnO_2.

The first charge/discharge curves of 1.2-MnO_2 and 3.6-MnO_2 electrodes at a current density of 100 mA g^{-1} are shown in Fig4(c). The initial discharge voltage profiles for both samples show a weaken voltage plateau around 2.23 V, a strong voltage drop from 2.23 to 0.44 V, and a long voltage plateau at 0.44 V. the voltage plateaus at 2.23 V and 0.44 V ascribed to the formation SEI layer and reduction of MnO_2 to Mn. In the initial charge profile, the potential plateau at 1.25 V corresponds to the oxidation of Mn to MnO_2. These results are in agreement with the CV results. Remarkably, the initial discharge capacities of two anode materials are 1321.3 mAh g^{-1} and 1515.1 mAh g^{-1}, respectively, significantly higher than that of the theoretical specific capacity of MnO_2, the additional capacity might result from the formation of SEI layer on the surface of MnO_2 and acetylene black[1, 24]. The initial charge capacity of the two electrodes are 522.2 mAh g^{-1} and 506.6 mAh g^{-1}, much

higher than 439 mAh g^{-1} of β-MnO_2 and 369 mAh g^{-1} of δ-MnO_2[25]. The high irreversible capacity fading of the electrodes are presumably attributed to the formation of solid electrolyte interface (SEI) layer and the decomposition of the electrolyte, which is a common drawback for the other transition metal oxides[26].

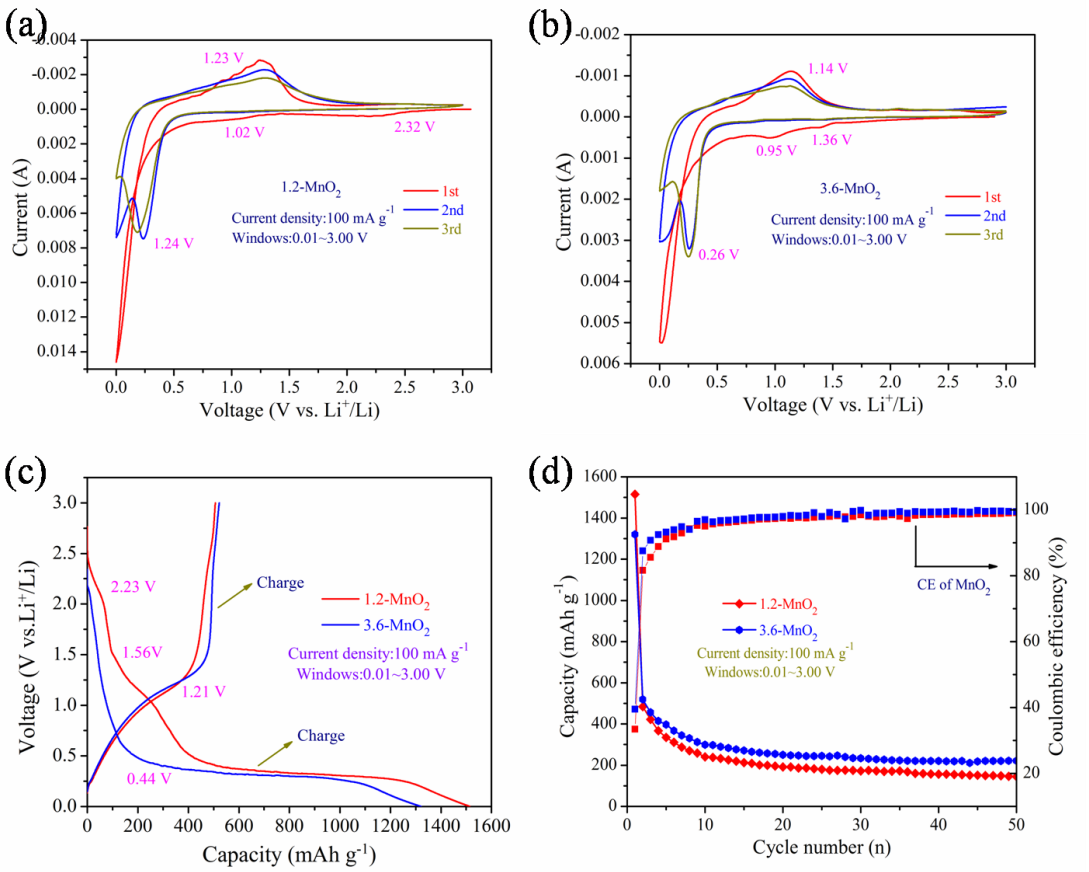

Figure 4. Electrochemical performance of the four MnO_2 electrodes: **(a)–(b)** First three CV curves of 1.2-MnO_2 and 3.6-MnO_2 at a scan rate of 0.2 mV s^{-1}, respectively, Charge/discharge curves **(c)** and cycling performance **(d)** of 1.2-MnO_2 and 3.6-MnO_2 at the current density of 100 mA g^{-1}.

The cycling performance and coulombic efficiency of the two anode materials are displayed in Fig4(d). From the Fig4(d), we can see both of the two samples show significantly fast capacity fading, which can be ascribed to the unavoidably cracking and pulverization of the active materials. Then the specific capacity slowly decreases after the first cycle, and finally these materials can maintain reversible capacities of 144.9 mAh g^{-1} and 221.4 mAh g^{-1} at the end of 50 cycles, with the capacity retention ration of 9.6% and 16.8%, respectively. Compare the cycling performance of the two materials, it is easily found that the 3.6-MnO_2 shows better performance than the 3.6-MnO_2 material, which due to it has a higher specific surface area that could improve the electron and Li^+ diffusion as well as provide large amount of electrochemical activated sites. During the first several cycles, all the two samples have relatively low coulombic efficiency. Then the coulombic efficiency significantly increases with increasing the cycle number and finally the coulombic efficiency can keeps more than 98%.

4. CONCLUSION

In this work, two different 1D α-MnO_2 anode materials have been successfully prepared through a facile and environmentally friendly hydrothermal method. It is clearly found that the solution acidity is significantly affected the morphology, size and specific surface area of the sample, and thus influence the electrochemical performance. The obtained MnO_2 electrodes exhibit high initial discharge capacity, and relatively excellent cycling stability. Compared to the 1.2-MnO_2, the 3.6-MnO_2 displays a better cycle performance. This difference might be due to the fact that the 3.6-MnO_2 sample with a relatively higher specific surface area and pore volume than 1.2-MnO_2, which could be short the electron and Li^+ diffusion, as well as enhance the Li^+ reaction sites.

ACKNOWLEDGEMENTS
This work was financially supported by Basic and Frontier Research Program of Chongqing Municipality (cstc2015jcyjA90020) and (cstc2014jcyjA10063) , Scientific and Technological Research Program of Chongqing Municipal Education Commission (KJ1501101), (KJ1500323) and (KJ1501116), China Postdoctoral Science Foundation (2015M582499), Postdoctoral special Foundation of Chongqing (Xm2015064) and Project of Chongqing Normal University (14XYY025) and (14XLB004), and National Natural Science Foundation of China (51502030).

References

1. N. Wang, X. Ma, H. Xu, L. Chen, J. Yue, F. Niu, J. Yang, Y. Qian, *Nano Energy*, 6(2014) 193-199.
2. J.-Y. Liao, D. Higgins, G. Lui, V. Chabot, X. Xiao, Z. Chen, *Nano Letters*, 13(2013) 5467-5473.
3. J. Ji, H. Ji, L.L. Zhang, X. Zhao, X. Bai, X. Fan, F. Zhang, R.S. Ruoff, *Adv Mater*, 25(2013) 4673-4677.
4. C. Chen, X. Hu, Z. Wang, X. Xiong, P. Hu, Y. Liu, Y. Huang, *Carbon*, 69(2014) 302-310.
5. Z. Bai, N. Fan, C. Sun, Z. Ju, C. Guo, J. Yang, Y. Qian, *Nanoscale*, 5(2013) 2442-2447.
6. C. Wang, Q. Li, F. Wang, G. Xia, R. Liu, D. Li, N. Li, J.S. Spendelow, G. Wu, *Acs Applied Materials & Interfaces*, 6(2014) 1243-1250.
7. H.B. Lin, H.B. Rong, W.Z. Huang, Y.H. Liao, L.D. Xing, M.Q. Xu, X.P. Li, W.S. Li, *Journal of Materials Chemistry* A, 2(2014) 14189-14194.
8. Y. Wang, P. Ding, C. Wang, *Journal of Alloys and Compounds*, 654(2016) 273-279.
9. X. Guo, J. Han, L. Zhang, P. Liu, A. Hirata, L. Chen, T. Fujita, M. Chen, *Nanoscale*, 7(2015) 15111-15116 .
10. Truong TT, Liu YZ, Ren Y, Trahey L, Sun YG, *ACS. Nano*. 9(2012) 8067-77.
11. X. Shen, T. Qian, J. Zhou, N. Xu, T. Yang, C. Yan, *Acs Applied Materials & Interfaces*, 7(2015) 25298-25305.
12. Y. Jiang, Z.-J. Jiang, B. Chen, Z. Jiang, S. Cheng, H. Rong, J. Huang, M. Liu, *Journal of Materials Chemistry* A, 4(2016) 2643-2650.
13. X. Zhang, T. Wang, C. Jiang, F. Zhang, W. Li, Y. Tang, *Electrochimica Acta*, 187(2016) 465-472.
14. H. Liu, J. Wang, *Electrochimica Acta*, 92(2013) 371-375.
15. L. Wang, K. Zhang, Z. Hu, W. Duan, F. Cheng, J. Chen, *Nano Research*, 7(2014) 199-208.
16. S. Deng, L. Wang, T.J. Hou, Y.Y. Li, *Journal of Physical Chemistry C*, 119 (2015) 28783-28788.
17. S. Xu, L. Lu, L. Liu, Y.-W. Luo, S.-Q. Wang, J.-W. Liu, G.-H. Li, C.-Q. Feng, *Chinese Journal of Inorganic Chemistry*, 32 (2016) 124-130.

18. D. Wang, L.M. Liu, S.J. Zhao, B.H. Li, H. Liu, X.F. Lang, *Physical Chemistry Chemical Physics*, *15 (2013) 9075-9083.*
19. H. Zhao, F. Liu, G. Han, Z. Liu, B. Liu, D. Fu, Y. Li, M. Li, *Journal of Solid State Electrochemistry*, 18(2014) 553-559.
20. G. Gnana Kumar, Z. Awan, K. Suk Nahm, J.S. Xavier, *Biosensors & bioelectronics*, 53(2014) 528-534.
21. M. Hu, K.S. Hui, K.N. Hui, *Chemical Engineering Journal*, 254(2014) 237-244.
22. Y.C. Dong, R.G. Ma, M.J. Hu, H. Cheng, C.K. Tsang, Q.D. Yang, Y.Y. Li, J.A. Zapien, *Journal of Solid State Chemistry*, 201(2013) 330-337.
23. L. Xing, C. Cui, C. Ma, X. Xue, *Materials Letters*, 65(2011) 2104-2106.
24. H. Ren, R. Yu, J. Wang, Q. Jin, M. Yang, D. Mao, D. Kisailus, H. Zhao, D. Wang, *Nano letters*, 14,(2014) 6679-6684.
25. H.D. Liu, J. Chen, R. Hu, X. Yang, H.B. Ruan, Y.Y. Su, W. Xiao, *Journal of Materials Science-Materials in Electronics*, 27 (2016) 3968-3973.
26. Wang P, Gao M, Pan H, Zhang J, Liang C, Wang J, Zhou P, Liu Y. *J. Power Sources*., 239(2013) 466-474